

STRUCTURAL PERFORMANCE OF RC BEAMS AND BEAM-COLUMN SUBASSEMBLAGES USING REINFORCEMENT WITH SLEEVE JOINTS AT THE END OF BEAMS

Yoshikazu TAKAINE¹, Satoru Nagai² and Makoto MARUTA²

¹Research Engineer, Kajima Technical Research Institute, Tokyo, JAPAN

²Chief Research Engineer, Kajima Technical Research Institute, Tokyo, JAPAN

Email: takaine@kajima.com, snagai@kajima.com, maruta@kajima.com

ABSTRACT:

A hinge relocation mechanism for reinforced concrete beams has been developed, using sleeve joints at the both ends. High-strength bars in the beam-column joint, and a high stirrup ratio near the sleeve joint produces a ductile hinge relocated beam. This ensures that beam bar yielding occurs at the sleeve tip before it occurs at the column face. Five beams and four beam-column subassemblages were tested, and their structural performance under earthquake conditions was confirmed. Recorded data showed that the ultimate strengths in flexure, shear, and bond-slipping, considering the evaluative length, could be calculated by conventional methods in these beams. The calculated skeleton curve and the hysteresis loop of shear force-rotation angle relationship, modified by considering the effect of stiffness increment at the sleeve joints, could roughly simulate the test results.

KEYWORDS: reinforced concrete, sleeve joint, hinge relocation beam, high stiffness beam, high strength beam

1. INTRODUCTION

Recently in Japan, a lot of tubular high-rise reinforced concrete (RC, hereafter) buildings have been constructed in preference to moment resisting frame RC buildings, because the tubular structure provides more flexible residential space with fewer columns and beams. Longer span beams are needed to realize this larger space. However, stiffness decreases as span increases, leading to reduced tube effect in the tubular structure system. Therefore, a new type of hinge relocation beam using sleeve joints (HiRBS, hereafter) based on the hinge relocation concept [1] has been developed, as shown in Figure 1. This type of beam has higher strength and higher stiffness than ordinary beams, thus enabling longer spans.

Ultra-high-strength mortar is cast in the sleeve joint to connect longitudinal bars of beam (beam bar, hereafter), as shown in Photo 1 and Figure 2. The use of high-strength beam bars in the beam-column joint, and a high stirrup ratio near the sleeve joint, produces a ductile hinge relocated beam. This ensures that beam bar yielding at the sleeve tip occurs prior to its yielding at the column face.

In this study, HiRBS beams and HiRBS beam-column subassemblages were tested to grasp structural performance,

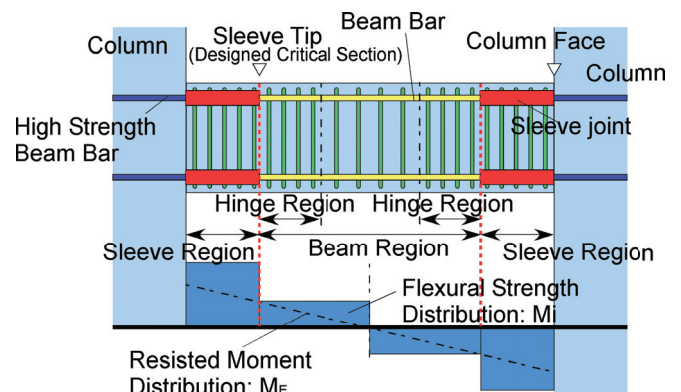


Figure 1 Concept of RC Beams using Sleeve Joints at the Ends of Beam



Photo 1 Sleeve Joint

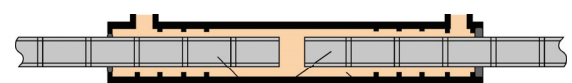


Figure 2 Detail of Sleeve Joint

and then methods for evaluating structural performance were discussed.

2. HINGE RELOCATION BEAM TEST

2.1. Outline of Test

Three HiRBS beams and two ordinary beams at 1/2.5 scale, with loading stubs at both ends were tested, as listed in Table 1. The specimen shape and bar arrangement are shown in Figure 3. The clear span length was fixed at 2000mm. The parameters of the test were 1) with or without sleeve joints (BN1 and BH1: ordinary beam, BT1 through BT3: HiRBS beam); 2) strength and quantity of bars (BN1: D19-SD490 $p_t=1.61\%$, BH1: D16-SD685 $p_t=1.12\%$, BT1 through BT3: D16-SD490 $p_t=1.12\%$, D: diameter, SD: specified yield strength (N/mm²), p_t : tension beam bar ratio); and 3) stirrup ratio P_w (0.36~1.66%).

All specimens were designed to show almost the same flexural strength. The ordinary beams and the HiRBS beams were designed for bar yielding at the stub faces and at the sleeve tips, respectively. For the HiRBS beams, to ensure that beam bar yielding occurred at the sleeve tips, the beam bar strength within the stubs was higher than that within the beam region (see Fig.1). BT1 through BT3 had different stirrup ratios, designed for flexural failure mode, share failure mode and bond splitting failure mode, respectively. For the ordinary beams, the beam bar diameter of BN1 was larger and the beam bar strength of BH1 was higher than that of the HiRBS beams, respectively.

The shear force was applied to the test portion, which was in double bending with a point of inflection at its midspan. According to the loading rule, reversed cyclic load was applied. The cyclic rule was determined by the rotation angle R. One loading cycle of R=0.125, two loading cycles of R=0.25, 0.5, 1.0, 2.0, 3.0, 4.0%, and R=10% were targeted.

2.2. Experimental Results

2.2.1 Outline of Test Result

Figure 4 shows the relationships between shear force and rotation angle. Table 2 lists the test results and various strength predictions, which were ultimate flexural strength calculated by the equivalent stress block according to ACI Code [2], ultimate shear strength and bond splitting strength according to AIJ, Architectural Institute of Japan, code [3]. For the HiRBS beams, the clear span length (2000mm) and the distance between sleeve tips (1530mm) were used for shear and bond splitting strength equations, respectively.

Flexural cracks occurred in all specimens before R reached 0.01rad. The first flexural cracks in ordinary beams occurred at the stub faces, while those in the HiRBS beams occurred at both the stub faces and the sleeve tips at almost the same time. Beam bar

Table 1 List of Specimens and material properties

Specimen	BN1	BH1	BT1	BT2	BT3
Sleeve	-		Sleeve Joint (Length: 240mm, Outer Diameter: 44mm)		
Section	285×500				
Clear Span	2000				
Beam Bar [p_t] (σ_y N/mm ²)	16-D19 SD490 [1.61%] (518.2)	16-D16 SD685 [1.12%] (737.6)	16-D16 SD490 [1.12%] (540.4)		
Stirrup [P_w] (σ_y N/mm ²)	Beam Region	2-D10 SD785 @80 [0.62] (888.8)	2-D10 SD785 @80 [0.62] (814.0)	2-D10 SD785 @140 [0.36] (814.0)	
	Hinge Region		4-D10 SD785 @60 [1.66] (814.0)		
	Sleeve Region		4-D10 SD785 @60 [1.66] (833.2)		
Concrete Strength (N/mm ²)	41.7	42.8	37.7	39.0	39.7

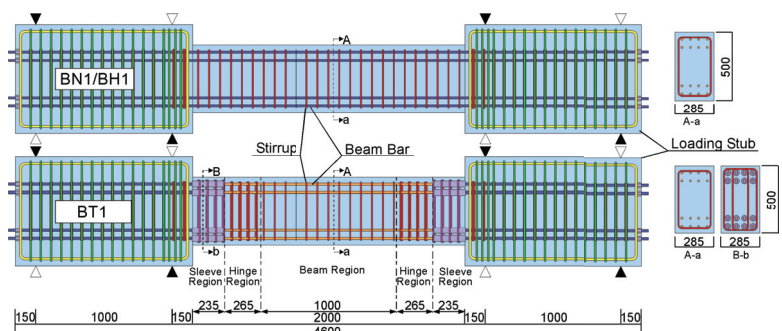


Figure 3 Shape and Bar Arrangement of Specimen

yielding occurred in the HiRBS beams earlier than in the ordinary beams (HiRBS beams: at the $R=0.01\text{rad}$ cycle, ordinary beams: at the $R=0.02\text{rad}$ cycle). This was because the deformable length of the HiRBS beams became shorter than the clear span length due to hinge relocation.

Finally, in BT1, BN1 and BH1, compressive crushing of concrete was observed around the sleeve tips (BT1) or at the column faces (BN1 and BH1), so failure mode was judged as flexure. In BT2, bond splitting cracks extended along the top beam bars, so failure mode was judged as bond splitting after flexural yielding. In BT3, shear crack width expanded and cover concrete spalled off, so failure mode was judged as shear after flexural yielding.

2.2.2 Cracking Behavior and Curvature Distribution

Photo 2 shows cracking patterns at $R=0.03\text{rad}$ and the final condition. In the HiRBS beams, a few wide flexural cracks at the sleeve tip portion and numerous flexural-shear cracks at the region $0.5D$ (D : the depth of the beam) from the sleeve tips were observed, extending to midspan direction.

Figure 5 shows the curvature distribution of flexural failure beams of BN1, BH1, and BT1 at each cycle peak. The curvature of the ordinary beams (BN1 and BH1) became large in the region $1.0D$ from the stub face toward midspan, particularly near the stub faces. However, the curvature of the HiRBS beam (BT1) became large in the region $0.5D$ from the sleeve tips toward midspan. Therefore, it was considered that a plastic hinge region was formed in the HiRBS beams at $0.5D$ from the sleeve tip and was shorter than that of the ordinary beams.

Table 2 List of Test Result

Specimen	Test Results							Calculated Strength							
	$Q_{fc}^{(1)}$ (kN)	$Q_{sc}^{(2)}$ (kN)	$eQ_{y2}^{(3)}$ (kN)	$eR_{y2}^{(4)}$ ($\times 10^{-3}\text{rad}$)	$eQ_m^{(5)}$ (kN)	$eR_m^{(6)}$ ($\times 10^{-3}\text{rad}$)	Failure Mode ⁷⁾	$cQ_{fu}^{(8)}$ (kN)	eQ_m cQ_{fu}	$cQ_{su}^{(9)}$ ($R_p=0.02$) (kN)	eQ_m cQ_{su}	cQ_{su} cQ_{fu}	$\tau_f^{(10)}$ (N/mm^2)	$0.8 \tau_{bu}^{(11)}$ (N/mm^2)	$\frac{0.8 \tau_{bu}}{\tau_f}$
BN1	33	144	450	11.3	479	30.1	F	448	1.07	631	0.76	1.41	3.12	3.72	1.19
BH1	33	144	450	13.5	472	20.1	F	439	1.08	631	0.75	1.44	3.73	4.44	1.19
BT1	33	141	370	6.8	478	20.1	F	432	1.11	764	0.63	1.77	3.89	4.17	1.07
BT2	33	140	379	7.8	476	20.1	FB	433	1.10	781	0.61	1.80		3.69	0.95
BT3	24	135	385	8.3	445	19.6	FS	434	1.03	319	1.40	0.73	3.72	0.96	

1) Flexural Crack Strength, 2) Shear Crack Strength, 3) Strength at Beam Bar Yielding of The Second Layer, 4) Rotation Angle corresponding to eQ_{y2} , 5) Maximum Strength, 6) Rotation Angle corresponding to eQ_m , 7) F: Flexural Failure, FB: Bond Splitting Failure after Flexural Yielding, FS: Shear Failure after Flexural Yielding, 8) Ultimate Flexural Strength, 9) Ultimate Shear Strength at $R_p=0.02\text{rad}$ (R_p : plastic rotation angle in the yield hinge region), 10) Design Bond Stress, 11) Bond Splitting Strength of Top Beam Bar

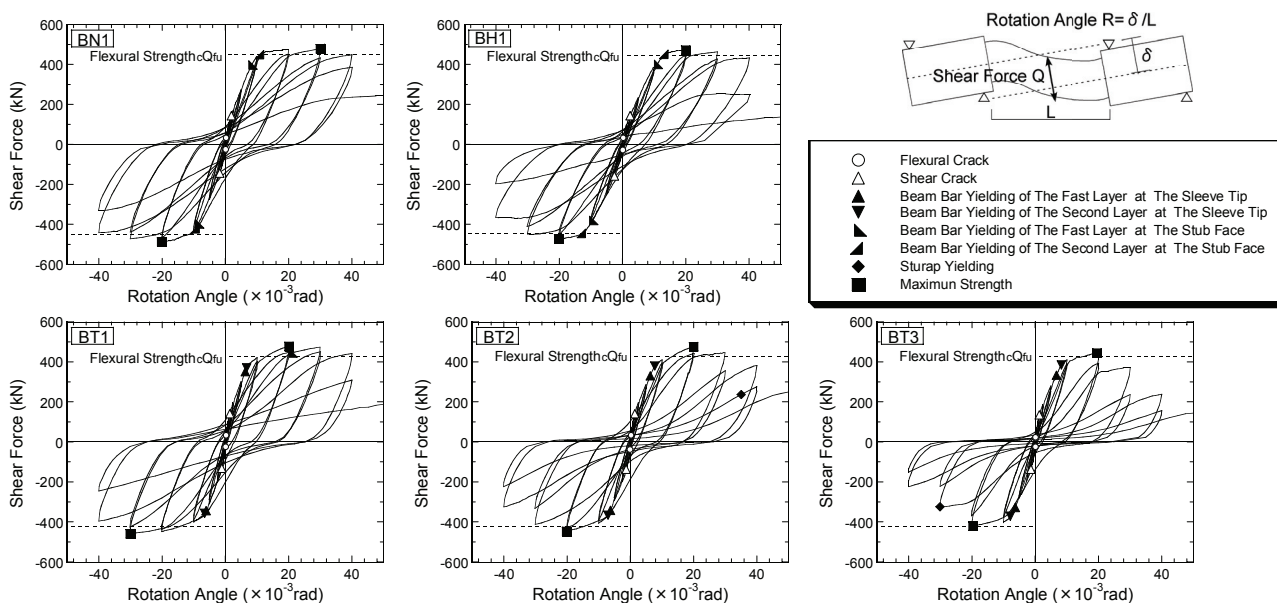


Figure 4 Shear Force and Rotation Angle Relationships

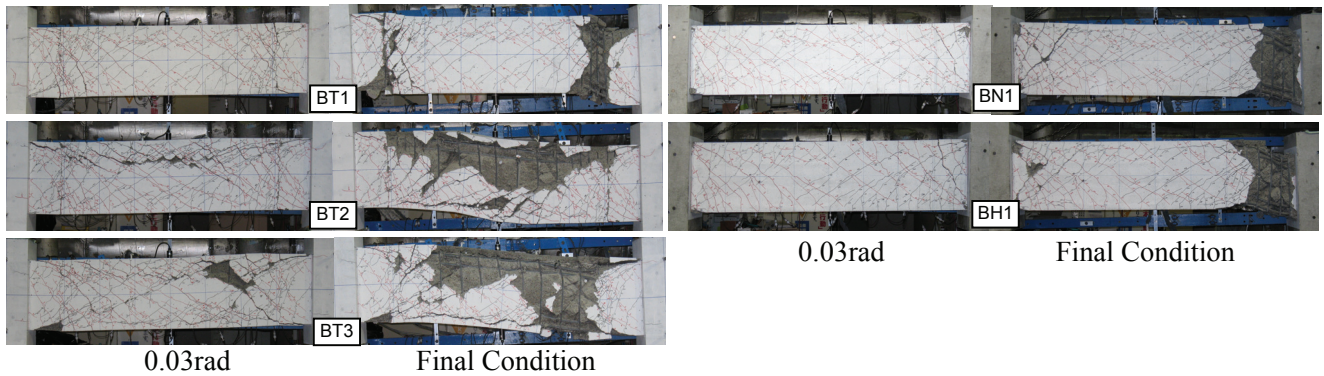


Photo 2 Damage Condition

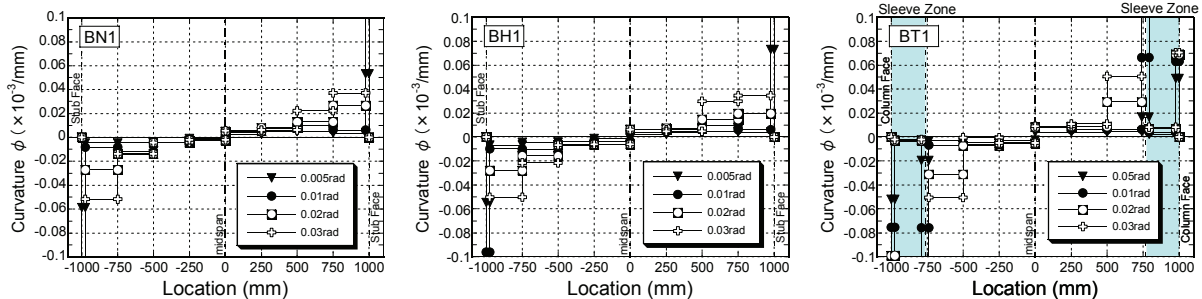


Figure 5 Curvature Distribution

2.2.3 Envelope Curves of Shear Force-Rotation Angle Relationship

Figure 6 shows envelope curves of shear force-rotation angle relationship for flexural failure beams (BN1, BH1, and BT1). The stiffness after cracking of BT1 was higher than that of BN1 and BH1 due to hinge relocation.

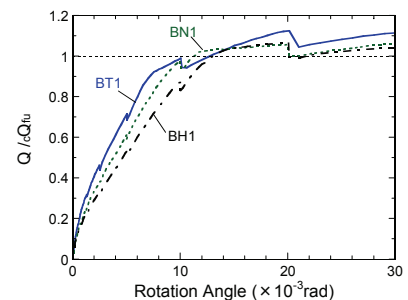


Figure 6 Envelope Curve

3. HINGE REROCATION BEAM-COLUMN SUBASSEMBLAGES TEST

3.1. Outline of Test

Table 3 lists four specimens and their material properties. Figure 7 shows the shape and bar arrangement of a typical specimen. The specimens consisted of four interior beam-column subassemblages at 1/2.5 scale. Three HiRBS beam specimens, JTU1 through JTU3, and one ordinary beam specimen, JH1, were tested. For the HiRBS beam specimens, to ensure that bar yielding occurred at the sleeve tips, the beam bar strength within the beam-column joint (joint panel, hereafter) was higher than that within the beam region. Beam of JTU1, JTU3 and JH1 was assumed to be reversed beam, and that of JTU2 was assumed to be a conventional beam, so its depth was different. The parameters of this test were 1) with or without sleeve joints at the beam ends; 2) beam depth (reversed beam: 500mm, conventional beam: 375mm); and 3) ratio of beam flexural strength ratio at the column face to that at the sleeve tip (JTU1: 1.29, JTU2 and JTU3: 1.04).

The column was supported by pins at each end, and a vertical reversed cyclic load was applied to the beam tips. The cyclic rule was determined by the story drift angle R_s . Two loading cycles of $R=0.125, 0.25, 0.5, 1.0, 2.0, 3.0, 4.0\%$, and $R=10\%$ were targeted.

3.2. Experimental Results

3.2.1 Outline of Test Result

Table 4 lists the experimental results and calculated strengths. Figure 8 shows the relationships between beam shear force and story drift angle. The ultimate flexural strengths of the beams were calculated by the equivalent stress block in the ACI Code [2].

Beam flexural cracks, column flexural cracks and joint panel shear cracks were observed in all specimens before $R_s=0.01\text{rad}$. In the HiRBS beam specimens, beam bar yielding occurred at the sleeve tips, and then obvious stiffness degradation was observed. Although beam bar yielding of the first layer at the column face occurred continuously, no obvious change of stiffness was observed. In the ordinary beam specimen, beam bar yielding occurred at the column face, and then obvious stiffness degradation was observed. The compressive concrete of the beam at the sleeve tips (HiRBS beam specimens) and at the column faces (ordinary beam specimen) was crushed at 0.02rad cycle peak. All specimens showed good flexural performance with high ductility, up to 0.04rad without degradation of beam shear strength. All specimens showed beam flexural failure mode.

3.2.2 Crack Behavior

Photo 3 shows the cracking patterns of JTU3 and JH1 at $R_s=0.02\text{rad}$ and 0.04rad. In JH1, wide flexural cracks were observed in the beams at the column faces. However, in JTU3, numerous fine flexural-shear cracks were observed in the beams at the 0.5D extent from the sleeve tip to beam tip direction near the sleeve tips. It is considered that, in JTU3, a plastic hinge region was formed at 0.5D from at the sleeve tip toward the beam tip.

The cracking pattern of both specimens at the joint panel was approximately the same at

Table 3 List of Specimens

Specimen	JTU1	JTU2	JTU3	JH1
Sleeve	Sleeve Joint (Length:240mm, Out of Diameter44mm)			-
Beam Section	285 × 500	285 × 375	285 × 500	
Beam Bar [Pt] (σ_y N/mm ²)	16-D16 SD490 [1.12%] (532.6)	16-D19 SD490 [2.15%] (532.9)	16-D16 SD490 [1.12%] (532.6)	16-D16 SD685 [1.12%] (738.7)
Beam Bar within Beam-Column Joint (σ_y N/mm ²)	16-D19 SD590 (626.6)	16-D19 SD685 (733.0)	16-D16 SD685 (738.7)	
Stirrup [Pw] (σ_y N/mm ²)	Beam Zone 2-D10SD785@60 [0.83%] Sleeve Zone and Hinge Zone 4-D10SD785@60 [1.66%] (888.0)			
Column Section	500 × 500			
Column Bar [Pg]	12-D19 SD490 [1.38%]	14-D19 SD490 [1.61%]	12-D19 SD490 [1.38%]	14-D19 SD490 [1.61%]
Hoop [Pw]	4-D10SD785 @80 [0.71%]			4-D10SD785 @70 [0.81%]
Hoop within Beam-Column Joint	2-D10SD785 @50			
Concrete Strength (N/mm ²)	Beam : 35.5 Column : 79.6	Beam : 35.2 Column : 80.8	Beam : 34.8 Column : 79.4	Beam : 35.1 Column : 78.3

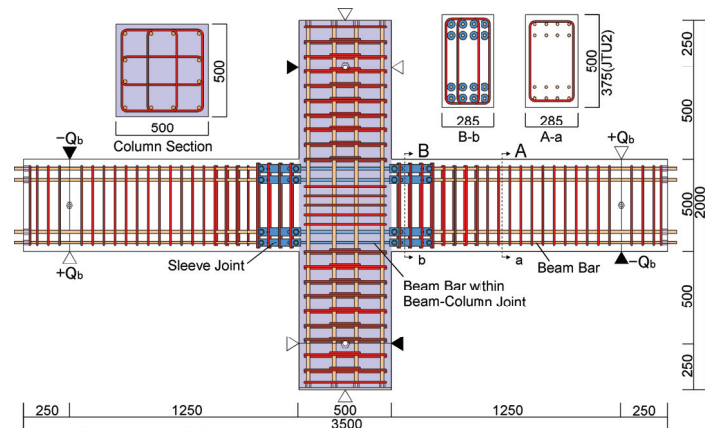


Figure 7 Shape and Bar Arrangement of a Specimen (JTU1)

Table 4 List of Test Result

Specimen	Test Results(Beam Tip Shear Force)					Calculation(Beam Tip Shear Force)					Failure Mode ¹⁰⁾		
	e-bQfc ¹⁾ (kN)	e-jQsc ²⁾ (kN)	eQy2 ³⁾ (kN)	eRy2 ⁴⁾ (x10 ⁻³ rad)	eQm ⁵⁾ (kN)	eRm ⁶⁾ (x10 ⁻³ rad)	c-bQfc ⁷⁾ (kN)	e-bQfc/c-bQfc	c-jQsc ⁸⁾ (kN)	e-jQsc/c-jQsc		c-bQfu ⁹⁾ (kN)	eQm/c-bQfu
JTU1	25.2	253.3	285.8	9.03	336.2	30.0	47.3	0.53	283.6	0.89	316.2	1.06	F
JTU2	18.1	175.8	269.2	15.67	312.7	97.7	26.3	0.69	170.8	1.03	292.8	1.07	F
JTU3	24.9	250.6	285.3	9.37	332.8	40.1	46.5	0.54	283.4	0.88	315.6	1.05	F
JH1	24.9	253.3	346.9	14.37	363.6	30.1	38.3	0.65	282.0	0.90	345.9	1.05	F

1) Flexural Crack Strength, 2) Shear Crack Strength, 3) Strength at Beam Bar Yielding off The Second Layer, 4) Rotational Angle corresponding to eQ_{y2} , 5) Maximum Strength, 6) Rotational Angle corresponding to eQ_m , 7) Flexural Crack of Beam, 8) Shear Crack of Beam-Column Joint, 9) Flexural Strength of Beam, 10) F: Beam Flexural Failure

$R_s=0.02\text{rad}$. However, many more shear cracks were observed at the joint panel in JH1 than in JTU3 at $R_s=0.04\text{rad}$.

3.2.3 Envelope Curves of Beam Shear Force-Story Drift Angle Relationships and Shear Stress-Shear deformation Relationships at the joint panel

Figure 9 shows envelope curves of beam shear force-story drift angle relationship for all specimens. The maximum strength of JTU1, JTU3 and JH1 were approximately the same, while the stiffness before beam flexural yielding of JTU1 and JTU3 were higher than that of JH1 due to hinge relocation.

The relationships between beam shear force and story drift angle of JTU1 and JTU3 showed approximately the same relationships, although the flexural strength ratio of the calculated strength at the column face to that at the sleeve tip were different.

Figure 10 shows the relationships between shear stress and shear deformation at the joint panel of JTU3 and JH1. Shear strengths at the joint panel, calculated by the AIJ formula [4], are also plotted. The joint panel was not so damaged, because the experimental shear stress at the joint panel was approximately half of the calculated shear strength. In JTU3, slight degradation of shear stiffness due to the occurrence of shear cracks at the joint panel was observed, and residual shear deformation was small. However, in JH1, obvious degradation of shear stiffness was observed, and then the hysteretic loop and residual shear deformation became gradually larger. The yielding area of beam bars of JH1 spread from the column face into the joint panel, hence bond deterioration occurred in bars of beams within a joint panel.

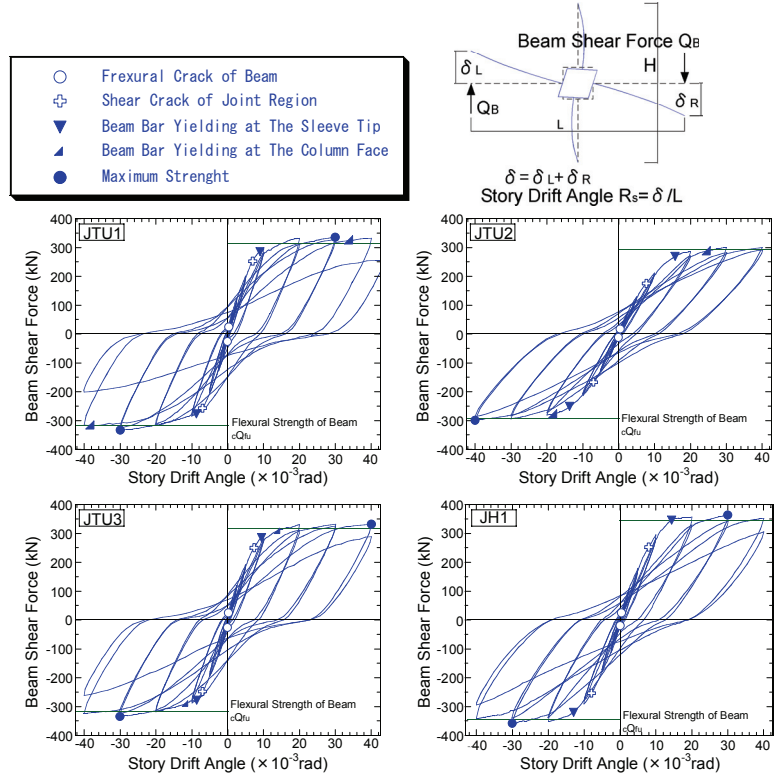


Figure 8 Beam Shear Force and Story Drift Angle Relationship

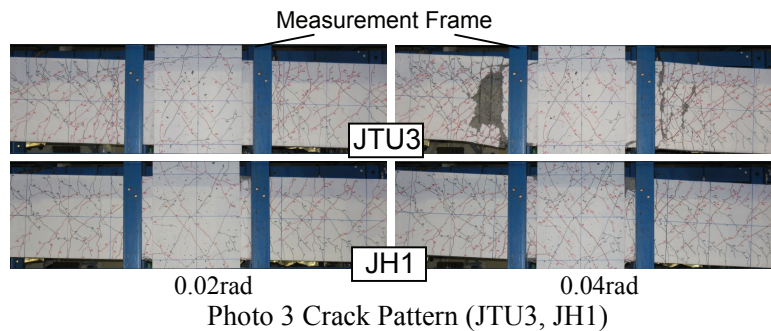


Photo 3 Crack Pattern (JTU3, JH1)

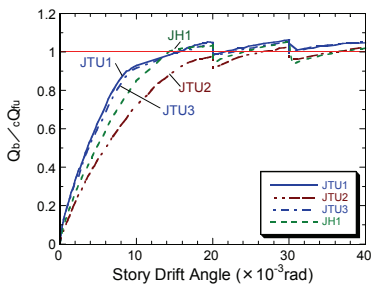


Figure 9 Envelope Curve

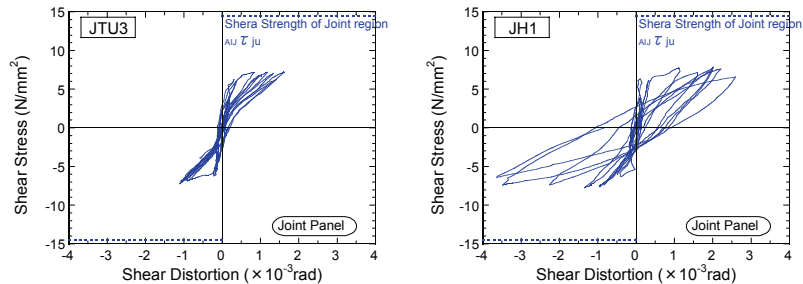


Figure 10 Relationships between Shear Stress and Shear Deformation at The Joint Panel

4. EVALUATION OF STRUCTURAL PERFORMANCE

4.1. Maximum Strength and Failure Mode

Table 2 and Table 4 list the test results and calculated values. eQ_m is the experimental maximum strength. cQ_{fu} is the beam flexural strength calculated by the ACI method. For the HiRBS beam, flexural strength was calculated at the sleeve tip. $cQ_{su(Rp=0.02)}$ was the calculated beam shear strength at $Rp=0.02$ rad (Rp : plastic rotation angle in the yield hinge region) by the AIJ formula [3]. Figure 11 shows the relationship between the ratio of eQ_m to cQ_{fu} and the ratio of $cQ_{su(Rp=0.02)}$ to cQ_{fu} . It is clear from this figure that the beam flexural strength calculated by the ACI method could predict the test results of HiRBS beams and HiRBS beam-column subassemblages.

Table 2 lists the design bond stress τ_f and the bond splitting strength $0.8\tau_{bu}$ for the top beam bars of the beam specimens, calculated by the AIJ formula [3]. Figure 12 shows the relationship between the ratio of $cQ_{su(Rp=0.02)}$ to cQ_{fu} and the ratio of $0.8\tau_{bu}$ to τ_{fu} . If these ratios were under 1, the specimens showed shear or bond splitting failure. Therefore, to prevent these failure modes, it was necessary for the ratio of $cQ_{su(Rp=0.02)}$ to cQ_{fu} and the ratio of $0.8\tau_{bu}$ to τ_{fu} to be over 1.

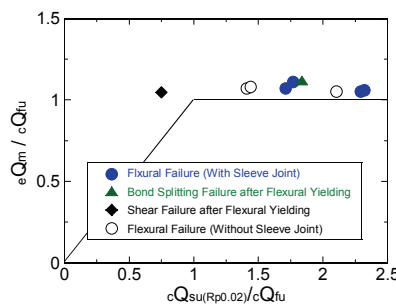


Figure 11 Flexural Strength

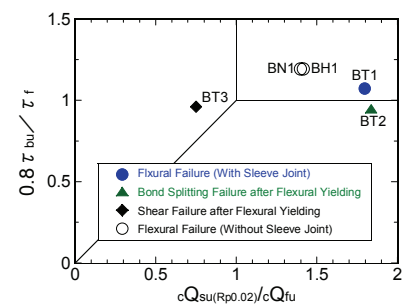


Figure 12 Failure Mode

4.2 Hysteresis Characteristics

In order to evaluate the hysteresis characteristics of the HiRBS beams and the HiRBS beam-column subassemblages, it was necessary to evaluate the effect of stiffness increment by sleeve joints. This paper proposed a hysteresis characteristic model considering this effect, as shown in Figure 13. The skeleton curve of beam, column and joint panel were assumed to be Tri-Linear. Their hysteresis loops were assumed to be Degrading Tri-Linear loops (Takeda model [6]).

The details of the suggested model were as follows. (1) Initial stiffness K_1 was calculated by flexural stiffness and shear stiffness for a beam and a column. When the total flexural stiffness of a HiRBS beam was calculated, flexural stiffness at sleeve region and beam region have to be considered. (2) Flexural crack strengths for a beam and a column were calculated by the AIJ formula [5]. (3) The degradation stiffness ratio α_y after flexural cracking were calculated by Sugano's equation [5]. In this calculation, the member length for a HiRBS beam should be each region's length. (4) Stiffness after flexural yielding

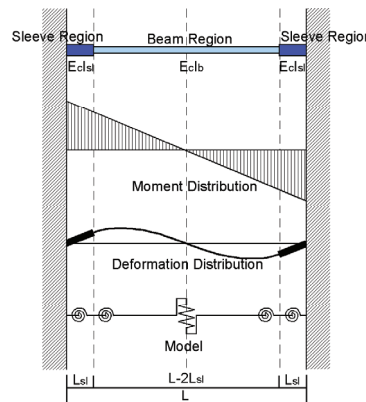


Figure 13 Hysteresis Characteristics Model

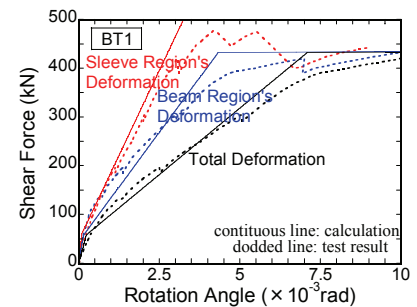


Figure 14 Verification of Hysteresis Model

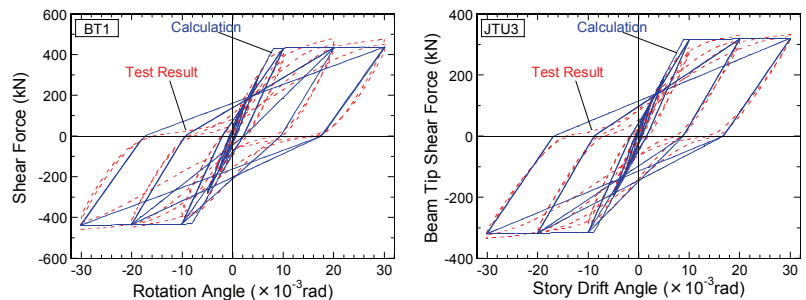


Figure 15 Relationships between the Hysteresis Characteristics Model and Test Results

was assumed to be $K_1/1000$. (5) For beam-column subassemblages, a skeleton curve of the joint panel was calculated by elastic shear stiffness up to shear cracking and one sixth of the elastic stiffness after shear cracking.

Figure 14 shows the relationships between the experimental envelope curve and the evaluated skeleton curve of BT1 with sleeve joints. In addition, experimental deformation was divided into beam region's deformation and sleeve region's deformation to confirm the accuracy of the evaluation method. In this calculation, flexural deformation of the beam region and sleeve region were calculated from measured curvature. The shear deformation, which was assumed to be total deformation minus total flexural deformation, was divided among regions considering each region's length. As a consequence, the calculated skeleton curve showed good correspondence with the experimental envelope curve before flexural yielding, but the stiffness of the calculated skeleton curve was higher than that of the obtained envelope curve near flexural yielding due to nonlinear shear behavior and slip out of beam bars from column faces and sleeve joints.

Figure 15 shows relationships between the hysteresis characteristics using the Takeda model and test results of BT1 and JTU3 with sleeve joints. The proposed method of skeleton curve and hysteresis characteristics using the Takeda model indicated good correspondence with the test results.

5. CONCLUSION

A hinge relocation mechanism for beams has been developed using sleeve joints at the both ends of a beam. A ductile hinge relocated beam has been formed by using high strength bars within the beam-column joint and a high stirrup ratio near the sleeve joint. Results of tests on these beams and beam-column subassemblages have been reported. The structural performance of a hinge relocated beam (HiRBS) has been compared to that of ordinary beams. The conclusions are as follows;

- 1) This mechanism ensures that beam bar yielding at the sleeve tip occurs before at the column face.
- 2) The stiffness before flexural yielding of a HiRBS beam is higher than that of an ordinary beam.
- 3) For the HiRBS, a few wide flexural cracks at the sleeve tip portion and numerous flexural-shear cracks at 0.5D from the sleeve tip toward the midspan direction are observed. The curvature in the 0.5D region is large when the rotation angle R is over 2% rad. Therefore, the region of 0.5D is indicated as the hinge length.
- 4) The ultimate strengths of the HiRBS in flexure, shear and bond-slipping have been calculated by the ACI and AIJ methods. However, the evaluative length has to be considered. The length for the shear calculation is defined between columns, and that for bond slipping calculation is defined between the sleeve tips.
- 5) The skeleton curve and the hysteresis loop, modified by considering the effect of stiffness increment at the sleeve joints, can roughly simulate the HiRBS test results.

REFERENCES

1. Paulay, T. and Priestley, M. J. N. (1992). Seismic design of reinforced concrete and masonry buildings, JOHN WILEY & SONS, INC.
2. American Concrete Institute. (2002). Building Code Requirement for Structural Concrete and Commentary. ACI 318-02/318R-02.
3. Architectural Institute of Japan. (1990). Design Guidelines for Earthquake Resistant Reinforced Concrete Buildings Based on Ultimate Strength Concept. (In Japanese)
4. Architectural Institute of Japan. (1997). Design Guidelines for Earthquake Resistant Reinforced Concrete Buildings Based on Inelastic Displacement Concept. (In Japanese)
5. Architectural Institute of Japan. (1999). AIJ Standard for Structural Calculation of Reinforced Concrete Structures Based on Allowable Stress Concept. (In Japanese)
6. Takeda, T., Sozen, M. and Nielsen, M. N. (1970). Reinforced concrete response to simulated earthquakes. ASCE. **96:ST12**, 2557-2573